



Ultrasensitive sensing in air based on graphene-coated hollow core fibers

MENG HUANG,^{1,3} CONGHAO YANG,^{2,3} BING SUN,^{1,*} ZUXING ZHANG,^{1,4} LIN ZHANG²

¹Advanced Photonics Technology Lab, College of Electronics and Optical Engineering & College of Microelectronics, Nanjing University of Posts and Telecommunications, Nanjing 210023, China

²Aston Institute of Photonic Technologies, Aston University, Birmingham B4 7ET, UK

³These authors contributed equally to this paper

⁴zxyzhang@njupt.edu.cn

*b.sun@njupt.edu.cn

Abstract: The mismatching between permittivities of guided mode and air limits the operation of accurately monitoring the change in the refractive index of the surrounding air. To solve it, we propose a platform using a hollow core fiber with the integration of graphene coating. Experimental results demonstrate that the anti-resonant reflecting guidance has been enhanced while it induces sharply and periodically lossy dips in the transmission spectrum. We conclude a sensitivity of -365.9 dB/RIU and a high detection limit of 2.73×10^{-6} RIU by means of interrogating the intensity of the lossy dips. We believe that this configuration opens a direction for highly sensitive sensing in researches of chemistry, medicine, and biology.

© 2018 Optical Society of America under the terms of the [OSA Open Access Publishing Agreement](#)

OCIS codes: (060.2340) Fiber optics components; (060.2270) Fiber characterization; (060.2370) Fiber optics sensors; (160.4236) Nanomaterials.

References and links

1. H. Liang, H. Miranto, N. Granqvist, J. W. Sadowski, T. Viitala, B. Wang, and M. Yliperttula, "Surface plasmon resonance instrument as a refractometer for liquids and ultrathin films," *Sens. Actuators B Chem.* **149**(1), 212–220 (2010).
2. C. Caucheteur, T. Guo, F. Liu, B. O. Guan, and J. Albert, "Ultrasensitive plasmonic sensing in air using optical fibre spectral combs," *Nat. Commun.* **7**, 13371 (2016).
3. A. Iadicco, S. Campopiano, A. Cutolo, M. Giordano, and A. Cusano, "Self temperature referenced refractive index sensor by non-uniform thinned fiber Bragg gratings," *Sens. Actuators B Chem.* **120**(1), 231–237 (2006).
4. Y. Tan, W. Ji, V. Mamidala, K. Chow, and S. Tjin, "Carbon-nanotube-deposited long period fiber grating for continuous refractive index sensor applications," *Sens. Actuators B Chem.* **196**(3), 260–264 (2014).
5. C. Liu, Q. Cai, B. Xu, W. Zhu, L. Zhang, J. Zhao, and X. Chen, "Graphene oxide functionalized long period grating for ultrasensitive label-free immunosensing," *Biosens. Bioelectron.* **94**(15), 200–206 (2017).
6. Z. Yan, Q. Sun, C. Wang, Z. Sun, C. Mou, K. Zhou, D. Liu, and L. Zhang, "Refractive index and temperature sensitivity characterization of excessively tilted fiber grating," *Opt. Express* **25**(4), 3336–3346 (2017).
7. Y. Wang, D. N. Wang, C. R. Liao, T. Hu, J. Guo, and H. Wei, "Temperature-insensitive refractive index sensing by use of micro Fabry-Pérot cavity based on simplified hollow-core photonic crystal fiber," *Opt. Lett.* **38**(3), 269–271 (2013).
8. Z. Li, Y. Wang, C. Liao, S. Liu, J. Zhou, X. Zhong, Y. Liu, K. Yang, Q. Wang, and G. Yin, "Temperature-insensitive refractive index sensor based on in-fiber Michelson interferometer," *Sens. Actuators B Chem.* **199**(4), 31–35 (2014).
9. B. Xu, Y. Liu, D. Wang, D. Jia, and C. Jiang, "Optical Fiber Fabry-Pérot Interferometer Based on an Air Cavity for Gas Pressure Sensing," *IEEE Photonics J.* **9**(2), 1–9 (2017).
10. Y. Zhao, F. Xia, and J. Li, Sensitivity-Enhanced "Photonic Crystal Fiber Refractive Index Sensor with Two Waist-Broadened Tapers," *J. Lightwave Technol.* **34**(4), 1373–1379 (2016).
11. T. Zhu, Y. J. Rao, Y. Song, K. S. Chiang, and M. Liu, "Highly Sensitive Temperature-Independent Strain Sensor Based on a Long-Period Fiber Grating With a CO₂-Laser Engraved Rotary Structure," *IEEE Photonics Technol. Lett.* **21**(8), 543–545 (2009).
12. Y. Ran, L. Jin, L. P. Sun, J. Li, and B. O. Guan, "Temperature-Compensated Refractive-Index Sensing Using a Single Bragg Grating in an Abrupt Fiber Taper," *IEEE Photonics J.* **5**(2), 7100208 (2013).
13. J. Huang, X. Lan, A. Kaur, H. Wang, L. Yuan, and H. Xiao, "Temperature compensated refractometer based on a cascaded SMS/LPFG fiber structure," *Sens. Actuators B Chem.* **198**(4), 384–387 (2014).

14. J. Sadeghi, A. H. Ghasemi, and H. Latifi, "A label-free infrared opto-fluidic method for real-time determination of flow rate and concentration with temperature cross-sensitivity compensation," *Lab Chip* **16**(20), 3957–3968 (2016).
15. W. Qian, C. Chan, C. Zhao, Y. Liu, T. Li, L. Hu, K. Ni, and X. Dong, "Photonic crystal fiber refractive index sensor based on a fiber Bragg grating demodulation," *Sens. Actuators B Chem.* **166–167**(6), 761–765 (2012).
16. B. Sun, Y. Huang, S. Liu, C. Wang, J. He, C. Liao, G. Yin, J. Zhao, Y. Liu, J. Tang, J. Zhou, and Y. Wang, "Asymmetrical in-fiber Mach-Zehnder interferometer for curvature measurement," *Opt. Express* **23**(11), 14596–14602 (2015).
17. J. Villatoro, V. P. Minkovich, and J. Zubia, "Locally pressed photonic crystal fiber interferometer for multiparameter sensing," *Opt. Lett.* **39**(9), 2580–2583 (2014).
18. D. J. Hu, J. L. Lim, M. Jiang, Y. Wang, F. Luan, P. P. Shum, H. Wei, and W. Tong, "Long period grating cascaded to photonic crystal fiber modal interferometer for simultaneous measurement of temperature and refractive index," *Opt. Lett.* **37**(12), 2283–2285 (2012).
19. X. Zhang, Y. Yu, C. Zhu, C. Chen, R. Yang, Y. Xue, Q. Chen, and H. Sun, "Miniature End-Capped Fiber Sensor for Refractive Index and Temperature Measurement," *IEEE Photonics Technol. Lett.* **26**(1), 7–10 (2014).
20. C. Liao, S. Liu, L. Xu, C. Wang, Y. Wang, Z. Li, Q. Wang, and D. N. Wang, "Sub-micron silica diaphragm-based fiber-tip Fabry-Perot interferometer for pressure measurement," *Opt. Lett.* **39**(10), 2827–2830 (2014).
21. F. Bonaccorso, Z. Sun, T. Hasan, and A. Ferrari, "Graphene photonics and optoelectronics," *Nat. Photonics* **4**(9), 611–622 (2010).
22. Y. Zhao, X. Li, X. Zhou, and Y. Zhang, "Review on the graphene based optical fiber chemical and biological sensors," *Sens. Actuators B Chem.* **231**, 324–340 (2016).
23. Y. Wang, C. Shen, W. Lou, and F. Shentu, "Polarization-dependent humidity sensor based on an in-fiber Mach-Zehnder interferometer coated with graphene oxide," *Sens. Actuators B Chem.* **234**, 503–509 (2016).
24. T. Ouyang, L. Lin, K. Xia, M. Jiang, Y. Lang, H. Guan, J. Yu, D. Li, G. Chen, W. Zhu, Y. Zhong, J. Tang, J. Dong, H. Lu, Y. Luo, J. Zhang, and Z. Chen, "Enhanced optical sensitivity of molybdenum diselenide (MoSe₂) coated side polished fiber for humidity sensing," *Opt. Express* **25**(9), 9823–9833 (2017).
25. R. Gao, D. Lu, J. Cheng, Y. Jiang, L. Jiang, and Z. Qi, "Humidity sensor based on power leakage at resonance wavelengths of a hollow core fiber coated with reduced graphene oxide," *Sens. Actuators B Chem.* **222**, 618–624 (2016).
26. Y. Wu, B. C. Yao, A. Q. Zhang, X. L. Cao, Z. G. Wang, Y. J. Rao, Y. Gong, W. Zhang, Y. F. Chen, and K. S. Chiang, "Graphene-based D-shaped fiber multicore mode interferometer for chemical gas sensing," *Opt. Lett.* **39**(20), 6030–6033 (2014).
27. B. C. Yao, Y. Wu, A. Q. Zhang, Y. J. Rao, Z. G. Wang, Y. Cheng, Y. Gong, W. L. Zhang, Y. F. Chen, and K. S. Chiang, "Graphene enhanced evanescent field in microfiber multimode interferometer for highly sensitive gas sensing," *Opt. Express* **22**(23), 28154–28162 (2014).
28. B. Yao, Y. Wu, Y. Cheng, A. Zhang, Y. Gong, Y. Rao, Z. Wang, and Y. Chen, "All-optical Mach-Zehnder interferometric NH₃ gas sensor based on graphene/microfiber hybrid waveguide," *Sens. Actuators B Chem.* **194**(4), 142–148 (2014).
29. C. Guan, S. Li, Y. Shen, T. Yuan, J. Yang, and L. Yuan, "Graphene-Coated Surface Core Fiber Polarizer," *J. Lightwave Technol.* **33**(2), 349–353 (2015).
30. L. Yang, T. Hu, A. Shen, C. Pei, B. Yang, T. Dai, H. Yu, Y. Li, X. Jiang, and J. Yang, "Ultracompact optical modulator based on graphene-silica metamaterial," *Opt. Lett.* **39**(7), 1909–1912 (2014).
31. S. Chugh, R. Mehta, N. Lu, F. D. Dios, M. J. Kim, and Z. Chen, "Comparison of Graphene Growth on Arbitrary Non-Catalytic Substrates using Low-Temperature PECVD," *Carbon* **93**, 393–399 (2015).
32. C. Yang, L. Yun, Y. Qiu, H. Dai, D. Zhu, Z. Zhu, Z. Zhang, K. Yu, and W. Wei, "Direct growth of a graphitic nano-layer on optical fibers for ultra-fast laser application," *RSC Advances* **7**(82), 52261–52265 (2017).
33. Z. Zhang, C. Liao, J. Tang, Y. Wang, Z. Bai, Z. Li, K. Guo, M. Deng, S. Cao, and Y. Wang, "Hollow-Core-Fiber-Based Interferometer for High-Temperature Measurements," *IEEE Photonics J.* **9**, 1–9 (2017).
34. R. R. Nair, P. Blake, A. N. Grigorenko, K. S. Novoselov, T. J. Booth, T. Stauber, N. M. Peres, and A. K. Geim, "Fine structure constant defines visual transparency of graphene," *Science* **320**(5881), 1308 (2008).
35. S. Zhu, S. Yuan, and G. Janssen, "Optical transmittance of multilayer graphene," *Europhys. Lett.* **108**(1), 17007–17010 (2014).
36. M. Hou, F. Zhu, Y. Wang, Y. Wang, C. Liao, S. Liu, and P. Lu, "Antiresonant reflecting guidance mechanism in hollow-core fiber for gas pressure sensing," *Opt. Express* **24**(24), 27890–27898 (2016).
37. P. E. Ciddor, "Refractive index of air: new equations for the visible and near infrared," *Appl. Opt.* **35**(9), 1566–1573 (1996).
38. B. Jiang, X. Lu, X. Gan, M. Qi, Y. Wang, L. Han, D. Mao, W. Zhang, Z. Ren, and J. Zhao, "Graphene-coated tilted fiber-Bragg grating for enhanced sensing in low-refractive-index region," *Opt. Lett.* **40**(17), 3994–3997 (2015).
39. B. Shuai, L. Xia, Y. Zhang, and D. Liu, "A multi-core holey fiber based plasmonic sensor with large detection range and high linearity," *Opt. Express* **20**(6), 5974–5986 (2012).
40. P. K. Ang, A. Li, M. Jaiswal, Y. Wang, H. W. Hou, J. T. L. Thong, C. T. Lim, and K. P. Loh, "Flow sensing of single cell by graphene transistor in a microfluidic channel," *Nano Lett.* **11**(12), 5240–5246 (2011).

41. B. Yao, C. Yu, Y. Wu, S. W. Huang, H. Wu, Y. Gong, Y. Chen, Y. Li, C. W. Wong, X. Fan, and Y. Rao, "Graphene-Enhanced Brillouin Optomechanical Microresonator for Ultrasensitive Gas Detection," *Nano Lett.* **17**(8), 4996–5002 (2017).

1. Introduction

Accurate information on the refractive index (RI) of gas contributes to obtaining the optical properties, concentration and scattering properties of gas. It is taken for granted that optical fiber sensors have become increasingly attractive due to their high sensitivity, low cost and compact size. Such optical fiber sensors for RI measurement can be based on surface plasmon resonance [1,2], fiber gratings [3–6] or interferometric theory [7–10], among which the temperature cross-sensitivity issue is crucial in practical applications. And it can be resolved according to the following two schemes. One solution is to adopt temperature compensation [11–14] or to utilize a kind of PCF with a small thermal-optic coefficient [15-16]. The other one takes advantage of sensing heads involving with different sensitivities to each of physical parameters, namely multi-parameter sensors, such as temperature and force sensor [17] temperature and refractive index sensors [18-19] and temperature and pressure sensor [20].

Graphene has attracted a great deal of attention with the self-polarization effect, large optical absorption and relative high nonlinearity and so on [21]. In special, graphene-based chemical or biological sensors take favor of the good biomolecules adsorption characteristics of the graphene [22]. Owing to its outstanding merits, the combination of graphene and optical fibers such as graphene-based fiber interferometers [23–26] and high-sensitivity graphene-coated microfibers [27-28] have also been reported.

In this paper, we propose and experimentally demonstrate graphene-coated hollow core fibers (HCFs), which can be used to simultaneously measure the RI and temperature of the surrounding air. Anti-resonant reflecting guidance (ARRG) in the cladding has been enhanced due to that the external surface of the HCF is coated with few-layer graphene. Then, it induces periodically lossy dips in the transmission spectrum. Owing to the tunable refractive index of graphene, minor change in the refractive index of the surrounding air can be measured by means of interrogating the transmission intensity of the lossy dip. The results show a sensitivity of -365.9 dB/RIU and a high resolution of 2.73×10^{-6} RIU. In addition, the temperature cross-sensitivity problem can be effectively resolved.

2. Device design and preparation

As shown in Fig. 1(a), the sensing structure consists of a hollow core fiber (HCF) and two single mode fibers (SMFs). It is worth noting that the proposed structure has the advantages of low cost and ease of fabrication. In our experiment, a well-cleaved HCF with a length of ~ 3 mm is spliced with SMFs by using a conventional fiber splicer (S183PM, Fitel). The HCF (Polymicro Technologies, TSP025150) is composed of an air core with an inner diameter of $20 \mu\text{m}$ and a ring cladding with a thickness of $53 \mu\text{m}$, and the scanning electron microscope (SEM) image for the cross section of the HCF is shown in the left inset of Fig. 1(a). We take advantage of sophisticated skills to avoid collapsing HCF in the procedure of splicing, as listed in Table 1. And the optical image for the splicing result is depicted in the right inset of Fig. 1(a).

Table 1. Optimized splicing parameters for a commercial fusion splicer (S183PM, Fitel)

Parameters	Units	Values
prefusion power	bit	standard-20
prefusion time	ms	50
overlap	μm	15
fusion power	bit	standard-25
fusion time	ms	300
offset	μm	-15

Furthermore, a full-vectorial beam propagating simulation with a wide-angle beam method in cylindrical coordinates and perfectly matched layer boundary conditions has been employed. It's easily found that the guided light satisfies this resonate condition and then leaks out of the cladding at the wavelength of 1526.3 nm. When the wavelength is around 1516.4 nm, the guided light can be confined in the air core.

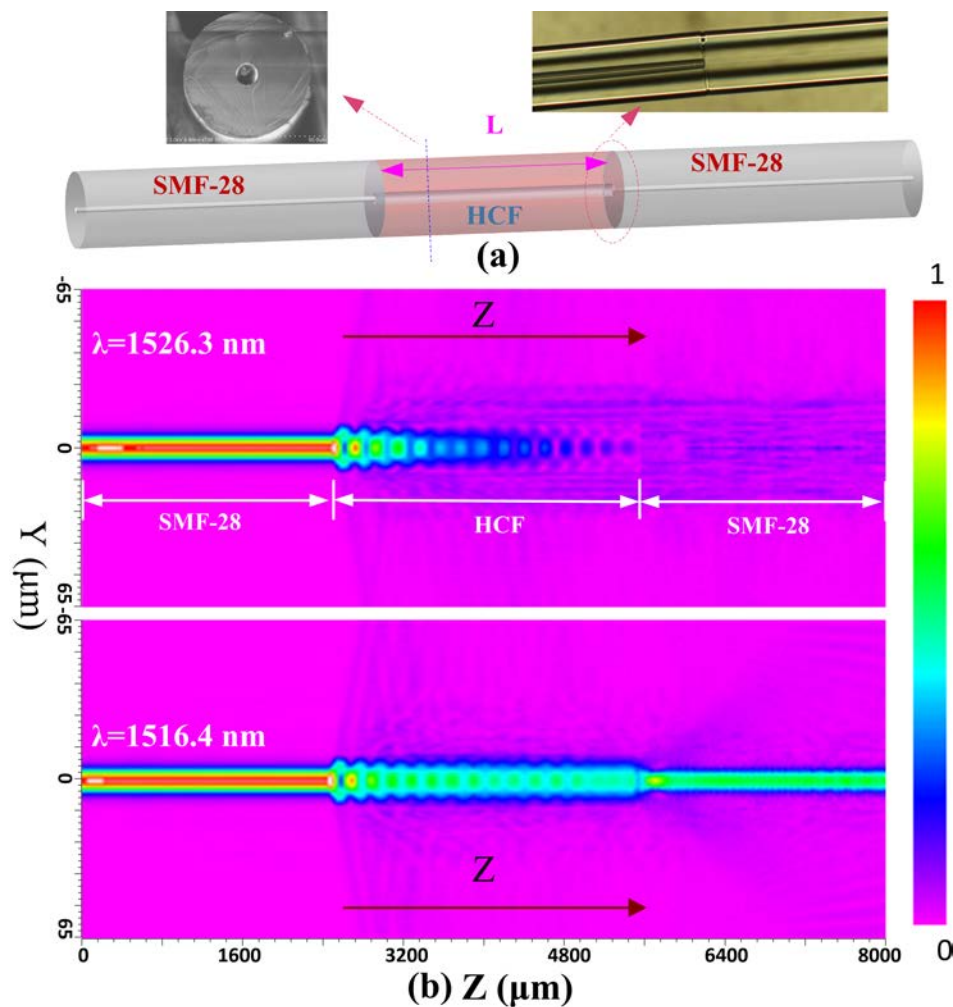


Fig. 1. (a) The optical image for the cross section of the hollow silica tube. The insets show the fiber splicing and the optical image for the cross section of the HCF. (b) Beam propagation simulation for the naked HCF sandwiched between SMFs at the wavelength of 1526.3 nm and 1516.4 nm, respectively.

It is well known that the optical guiding mechanism of the naked HCF can be explained according to the ARRG model, that is to say, it can be considered as a Fabry-Perot resonator, as shown in Fig. 2. When the wavelength locates at a particular resonance the ring cladding layer becomes transparent and light escapes from the core. As a result, it comes into being a transmission minimum. On the contrary, the anti-resonant wavelength contributes to a transmission maximum. As a result, periodic and narrow minimum and maximum appear in the whole transmission spectrum. The resonant wavelengths λ_m can be expressed as follows:

$$\lambda_m = \frac{2d_2}{m} \sqrt{n_1^2 - n_0^2} \quad (1)$$

where m is the resonance order, d_2 is the thickness of the cladding. And the refractive indices of the core and the ring cladding are defined as n_0 and n_1 , respectively.

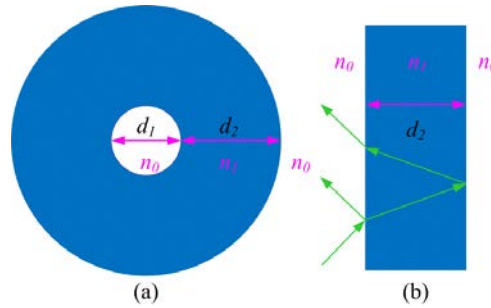


Fig. 2. (a) Schematic diagram for the cross section of the naked HCF. (b) Guiding mechanism of the naked HCF.

The complex refractive index (n_{eff}) of the graphene can be deduced from the dynamic conductivity (σ) of the graphene described by Kubo formula, which consists of the intraband and interband contributions [29-30].

$$n_{eff} = (1 + i \times \frac{\sigma}{\omega \Delta \epsilon_0})^{1/2} = 1 - \frac{\sigma_i}{\omega \Delta \epsilon_0} - i \times \frac{\sigma_r}{\omega \Delta \epsilon_0} \quad (2)$$

Where $\Delta = 782$ nm is the thickness of graphene, $\epsilon_0 = 8.85 \times 10^{-12}$ F/m, σ_i is the image part of σ , and σ_r is the real part of σ . And σ can be calculated through:

$$\begin{aligned} \sigma(\omega, \mu_c, \Gamma, T) &= \sigma_{intra} + \sigma_{inter} \\ &= \frac{-ie^2}{\pi \hbar^2 (\omega + i2\Gamma)} \left[\int_0^\infty \epsilon \left(\frac{\partial f_d(\epsilon)}{\partial \epsilon} - \frac{\partial f_d(-\epsilon)}{\partial \epsilon} \right) d\epsilon \right] + \frac{-ie^2 (\omega + i2\Gamma)}{\pi \hbar^2} \left[\int_0^\infty \frac{f_d(-\epsilon) - f_d(\epsilon)}{(\omega + i2\Gamma)^2 - 4(\epsilon/h)^2} d\epsilon \right] \end{aligned} \quad (3)$$

Where $f_d(\epsilon) = 1 / \exp((\epsilon - \mu_c) / \kappa_B T + 1)$ is the Fermi-Dirac distribution (κ_B is Boltzmann constant), $\hbar = h / 2\pi$ is the reduced Planck constant, ω is the angular frequency of the light wave, Γ represents the scattering rate, μ_c stands for the chemical potential and T is the temperature. When the graphene is coated on the external surface of the HCF, the light transmission corresponding to the resonant condition can be expressed as follows:

$$T_{resonant} = \frac{(1 - rr')^2 (r + r')^2}{1 + r'^4 - 2r'^2} I_{resonant}^i \quad (4)$$

Where $T_{resonant}$ is the transmission energy at the resonant wavelength, $I_{resonant}^i$ is the input light intensity at the resonant wavelength. r and r' are the reflection coefficients of the incident light at the core-cladding interface and the cladding-graphene interface, respectively. Significantly, the graphene coating changes the boundary condition of the fiber, the reflection coefficient r' is tuned simultaneously. Compared with the Fabry-Perot resonator without graphene, the graphene coating allows more light confined by the cladding leaking into the surrounding medium, and then the distribution of the evanescent field and spectral properties can be obviously modulated [25].

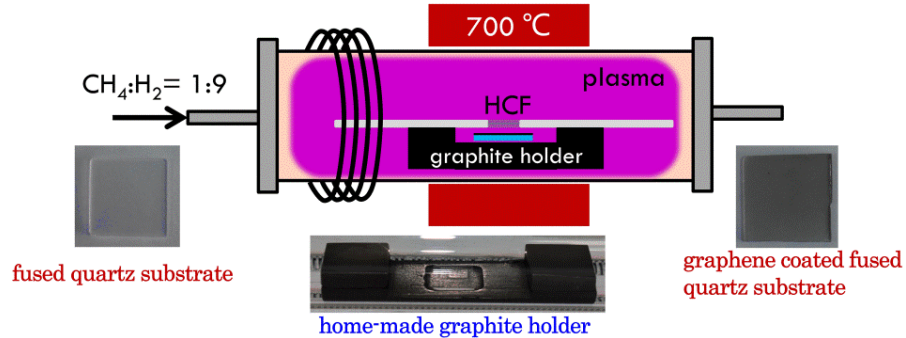


Fig. 3. The operation system of the employed PECVD.

The graphene was grown on fibers by using radio-frequency plasma enhanced chemical vapor deposition technique (RF-PECVD) [31-32]. As shown in Fig. 3, the operation system consisted of a tube furnace (OTF-1200X) and a generator (VERG-500 RF POWER GENERATOR, $f = 13.56$ MHz). On one hand, the HCF and fused quartz slide were placed side by side on a home-made graphite holder. Prior to the placement, the HCF and fused quartz substrate (size: 1.5×1.5 cm², thickness: 1 mm) were immersed in acetone and isopropanol solution, respectively, and then rinsed with deionized water. The reaction chamber was evacuated to ~ 40 mTorr while a mixture of methane and hydrogen gases ($\text{CH}_4:\text{H}_2 = 1:9$ sccm, standard cubic centimeter per minute) was introduced into the chamber when the reactor was heated up to 700 °C. In fact, the temperature of the reactor is flexible. And it's worth noting that the glass fiber can withstand extremes of temperature [33]. And the growth was conducted with a radio-frequency power of 200 W for 40 min. Thus, we turned off hydrogen valve, methane valve and plasma generator after the growth. Finally, we turned on the argon valve until the reactor fell to room temperature.

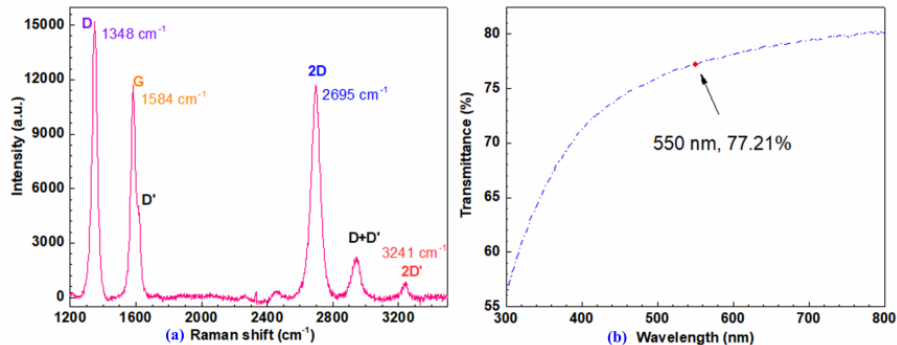


Fig. 4. (a) Raman scattering spectrum and (b) Optical transmittance of graphene coated fused quartz substrate.

The morphology and quality of the graphene grown on the surface of the fiber can be attained by means of carrying out Raman spectroscopy (EZM-785-A2, $\lambda = 532$ nm). As shown in Fig. 4(a), locations of three distinct peaks are 1348 cm^{-1} (D band), 1584 cm^{-1} (G band) and 2695 cm^{-1} (2D band), respectively. Owing to sp^2 -hybridized carbon-carbon bonds, the G and 2D bands indicates the formation of graphitized structure. The D band together with 2D band (3241 cm^{-1}) contributes to the structural disorder. The intense D band reveals small crystalline with numerous open edges and defects in the growth process. Furthermore, the layer number of graphene grown on the surface of the HCF can be achieved by means of measuring optical transmittance of graphene grown on the fused quartz substrate, which is placed together with the HCF. And optical transmittance of the graphene coating on quartz substrate is measured with a PerkinElmer Lambda 950 machine, as shown in Fig. 4(b). When the thickness of graphene is thin, its optical transmittance can be evaluated by a formula [34]:

$$T = 1 - \pi\alpha N \quad (5)$$

Where α is the fine-structure constant ($\sim 1/137$) [35], T is optical transmittance of the graphene film at the wavelength of 550 nm, and N is the layer number of graphene. As a result, N is calculated to be about 10 corresponding to $T = 77.21\%$. Hence concludes that the surface of the HCF is also coated with ten layers of graphene. It should be noted that N is just an equivalent value for the purpose of estimating the thickness of graphene, in fact the thin graphene film involving with a larger number of nano-platelets stacking together is beyond the scope of this article.

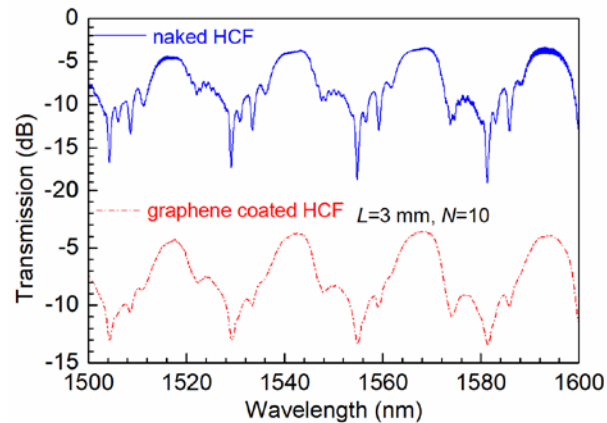


Fig. 5. Transmission spectra of the naked HCF and graphene coated HCF for $L = 3$ mm, $N = 10$.

We employ a wideband light source (1250nm-1650nm, Shenzhen Fiber lake Technology Co., Ltd.) and an optical spectrum analyzer (OSA, Yokogawa AQ6370C) to investigate the evolution of the transmission spectra. Firstly, we fabricate a compact structure with $L = 3$ mm, $N = 10$ to evaluate its performance, as shown in Fig. 5. Obvious inter-mode interference can be observed in the naked HCF, while the graphene coverage can flatten them well. Gao et al. [25] attributed it to the nonuniformity of the ring cladding thickness at different locations in the naked HCF. And Hou et al. [36] further found that the anti-resonant reflecting effect was due to the low reflectivity on the outer surface of the HCF. However, we deduce that the transmission spectra of the naked HCF include other periodic components.

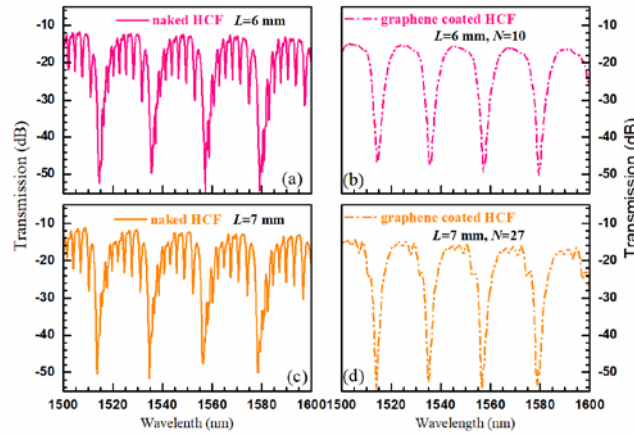


Fig. 6. (a-d) Transmission spectra of the naked HCF and graphene-coated HCF with different parameters.

To further estimate the effect of the sensor structures for L , another two samples with $L = 6$ mm and $L = 7$ mm are also fabricated. As shown in Figs. 6(a) and 6(c), it's obvious that the insertion loss increase with L due to the ARRG model would induce loss [36]. By contrast, higher-order periodic components are also obvious when the length of HCF increases. As a result, the interference is improved after graphene coating and the corresponding results are illustrated in Figs. 6(b) and 6(d). We tend to believe that the high-quality graphene fabricated by the PECVD contributes to exciting the dominating anti-resonant reflecting mechanism while suppressing another higher-order anti-resonant reflecting effect while it's acceptable that the graphene coverage actually weakens the extinction ratio. Furthermore, the multilayer graphene coating shows a little worse performance, as illustrated in Fig. 6(d).

3. Experimental results and discussion

The air pressure responses and hence to the refractive index of the proposed sensors ($L = 3$ mm, $N = 10$) are tested at a pressure chamber. The air pressure can be provided by a commercial pressure generator (ZC-YFT-02Q) with a stability of ± 0.2 kPa. To achieve an accurate pressure, a high-precision pressure meter is employed. In this experiment, the applied gas pressure in the chamber is increased from 0.1 MPa to 1.7 MPa with a step of 0.4 MPa by twisting the handle. Prior to each test, the pressure is maintained for 5 min. The raw data is used to calculate the sensitivity as a function of the surrounding refractive index. It should be noted that the refractive index of air is dependent on the atmospheric pressure and the temperature as follows:

$$n = 1 + (n_s - 1) \frac{p}{p_s} \frac{T_s}{T} \quad (6)$$

where $n_s = 1.00026825$, $P_s = 101325$ Pa and $T_s = 288.15$ K [37]. From this equation, we can find that the RI of ambient air has a linear relationship to the pressure at a given temperature. When the pressure increased from 0.1 Mpa to 1.7 Mpa, the RI of ambient air changed from 1.00026 to 1.00461. Figure 7(a) displays the corresponding evolution of the transmission spectra as a function of the surrounding refractive index. As shown in Fig. 7(b), a linear fitting of the raw data yields a sensitivity of $S_1^{dB} = 365.9$ dB/RIU, which is dozens of times larger than that of the reported intensity-modulated RI sensors [15], and three or four times larger than results reported in [17-18]. Jiang et al. proposed a method to significantly extend the sensitive window of tilted fiber-Bragg grating into low-refractive-index region with the

integration of graphene coating [38]. Moreover, the wavelength-modulated sensitivity is as low as $S_1^\lambda = 17.9 \text{ pm/RIU}$, which is shown in Fig. 7(c).

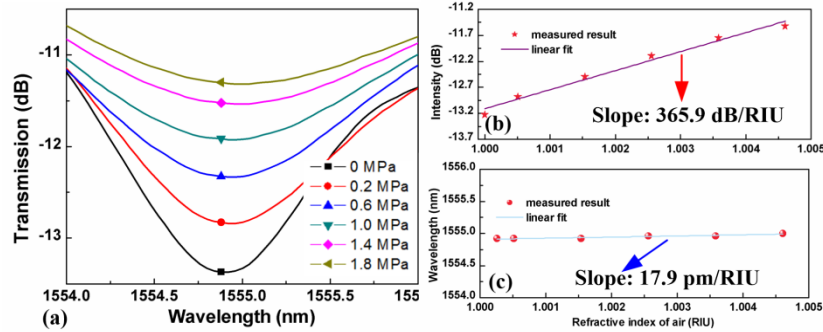


Fig. 7. (a) Transmission spectra of the sensor at different pressure. (b) Intensity and (c) wavelength shift correspond to the applied pressure.

The temperature response of the proposed sensor ($L = 3 \text{ mm}$, $N = 10$) has been investigated by placing it into a temperature-controlled oven, which increases the temperature from $30 \text{ }^\circ\text{C}$ to $100 \text{ }^\circ\text{C}$ with a step of $10 \text{ }^\circ\text{C}$. Figure 8(a) shows the transmission spectra with respect to the temperature, where a red shift (around 1555 nm) is clearly observed when the temperature increases. The wavelength shift is recorded and a linear sensitivity of $S_1^\lambda = 17.2 \text{ pm}/^\circ\text{C}$ can be concluded from Fig. 8(b). Furthermore, the dip (around 1555 nm) intensity presents hardly changes with the temperature and the sensitivity is demonstrated to be $S_1^{\text{dB}} = 0.011 \text{ dB}/^\circ\text{C}$. As a result, the temperature-induced RI measurement error is less than 3.01×10^{-5} without temperature compensation, which is ten times lower than that of the RI sensor reported in [23].

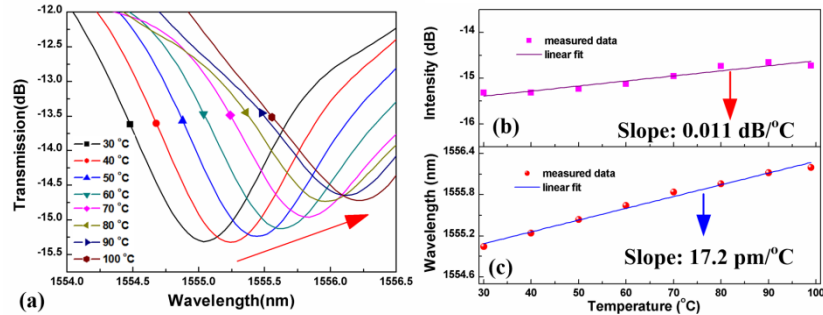


Fig. 8. (a) Transmission spectra of the sensor at different temperature. (b) Intensity and (c) wavelength shift correspond to temperature.

As shown in Fig. 7(b), the dip (around 1555 nm) intensity of interference fringes decreases but its shift shows hardly change with the surrounding RI. And the dip intensity of interference fringes also shows no evident change with the surrounding temperature. As a result, the proposed graphene-coated HCF can be used to develop a promising intensity-modulated and temperature-insensitivity RI sensor, which overcomes the temperature cross-sensitivity problem in the practical applications. More importantly, our proposed RI sensor exhibits a high sensitivity of -365.9 dB/RIU at the refractive index of air. Provided an optical spectrum analyzer with a resolution of 0.001 dB [39], a high RI resolution of $2.73 \times 10^{-6} \text{ RIU}$ can be achieved despite graphene based SPR [40] or ultra-high Q resonator [41] may be 10^{-8}

RIU level. However, graphene based optical structures with well field confinement are sensitive to local RI and ease to fabricate.

4. Conclusion

A novel graphene-coated HCF is demonstrated to accurately monitor the change in the refractive index of air. The length of the HCF is chosen as ~ 3 mm in order to achieve a large fringe contrast (as high as 15 dB). Such a compact structure presents a high sensitivity (-365.9 dB/RIU). In addition, the proposed RI sensor also exhibits the advantages of simple structure, easy fabrication and good repeatability.

Funding

National Natural Science Foundation of China (61505119, 61405125, 61425007); National Postdoctoral Program for Innovative Talents (BX201600077); Brain Gain Foundation of Nanjing University of Posts and Telecommunications (NY215040); and the Key Laboratory of Optoelectronic Devices and Systems of Ministry of Education and Guangdong Province (GD201706).

Acknowledgments

The authors thank Dr. Kehan Yu for providing technical support during graphene fabrication.